Mechanics of Materials 129 (2019) 1–14

Contents lists available at ScienceDirect

Mechanics of Materials

journal homepage: www.elsevier.com/locate/mechmat

Image analysis and the finite element method in the characterization of the influence of porosity parameters on the mechanical properties of porous EVA/PMMA polymer blends

Nataša Z. Tomić[a,*], Predrag Milanović[b], Bojan Međo[b], Marija M. Vuksanović[a], Đorđe Veljović[b], Marko Rakin[b], Radmila Jančić Heinemann[b]

[a] Innovation Center of the Faculty of Technology and Metallurgy, University of Belgrade, Karnegijeva 4, 11070 Belgrade, Serbia
[b] Faculty of Technology and Metallurgy, University of Belgrade, Karnegijeva 4, 11070 Belgrade, Serbia

ARTICLE INFO

Keywords:
Porous materials
Voronoi diagram
Delaunay triangulation
Hausdorff dimension
FEM
Parametric study

ABSTRACT

Poly(ethylene-*co*-vinyl acetate) (EVA) and poly(methyl methacrylate) (PMMA) are two incompatible polymers. Compatibilization of EVA/PMMA polymer blends with EVA-*g*-PMMA decreased the pore diameter and improved the mechanical properties. Image analysis of SEM micrographs enabled statistical analysis of the porosity parameters, including data about their positions. Positioning of the pores on the image was achieved by implementation of Voronoi diagrams and Delaunay triangulation by Python libraries. Hausdorff dimension (DH_f) analysis showed improved complexity of the material network obtained by compatibilization. The coordinates of pore contours were processed by the Ramer–Douglas–Peucker algorithm (RDP) to establish the models by the finite element method (FEM). This process is iterative and enables a parametric study of the problem so that the type of pore geometry responsible for the observed mechanical behavior could be revealed. The FEM revealed the regions of the material that bear the load and enabled the extraction of parts of the material that diminish the porosity but do not participate in load carrying. A parametric study showed a decrease of 22% in the maximal shear stress when the porosity increased 10%, suggesting the importance of bulging of the material that played the role in decreasing the porosity of non-bearing material. A procedure for selecting the model with a regular pore shape and distribution based on the actual (irregular) porous microstructure is proposed.

1. Introduction

Polymer blends are most used in the production and development of novel materials with unique properties (Visakh et al., 2016). Immiscibility of polymers in polymer blend contribute to increased porosity and thus decreased mechanical properties (Dimitrova et al., 2000; Tomić et al., 2017).When two polymers are mixed in a polymer blend they gain an arrangement of the phases representing a microstructure (Tucker III and Moldenaers, 2002).

Polymers are important materials as they have numerous uses and their mechanical properties can be influenced both by the composition and, in the case of similar compositions of two polymeric materials, by the microstructure. Critical microstructural parameters that affect the mechanical properties of the material are the values related to porosity, such as pore content and diameter, and complexity and arrangement of the pores. Critical parameter determination can lead to the design of a material having the desired mechanical properties. Polymer blends are used when one single polymer fails to achieve all the properties desired for a specific application. Hence, EVA copolymer was modified using PMMA and thus, polymer blend were obtained that enabled the mechanical properties to be modified. Microstructural analysis of these polymer mixtures led to the development of a tool for examining the microstructure and a correlation of the structural parameters to the mechanical behavior of a material under stress. Determination of the influence of critical parameters on the mechanical properties of a material based on EVA/PMMA polymer blend appeared to be crucial for establishing a functional material by modification and compatibilizing of the polymer blend. Image analysis is a useful tool in evaluating the microstructure parameters, such as pore area, diameters, coordinates of pore center, and ligaments length (Tomić et al., 2014). Correlation of these parameters with the obtained mechanical properties enable a prediction of the mechanical behavior of porous materials and thus to design materials according to the requirements of the mechanical characteristics.

* Corresponding author.
E-mail address: ntomic@tmf.bg.ac.rs (N.Z. Tomić).

https://doi.org/10.1016/j.mechmat.2018.10.008
Received 11 January 2018; Received in revised form 8 October 2018; Accepted 22 October 2018
Available online 23 October 2018
0167-6636/

All porous materials have a three dimensional structure that is observed mainly using their cross section and extrapolating such observations to the behavior of the material in exploitation. In two-dimensional images of heterogeneous materials, fractal geometry has been successfully used to describe the porous structure and surface irregularities (Jiao et al., 2014; Krohn and Thompson, 1986). There are many ways to quantify the pore shape by the fractal dimension of an SEM photograph, such as the box-counting method, the Fourier method and the probability statistics method (Keller et al., 1989; Xie and Wang, 1999). In this paper, the most popular method of box-counting (Hausdorff dimension) was applied.

Delaunay triangulation is used to describe structures composed of different mixtures of materials and to visualize and characterize the separated phases in the material. In porous materials, this method is used to characterize a local pore space in a coupled evolution of a solid grain (Russell et al., 2016). Combination of ubiquitous Voronoi–Delaunay tessellation is mostly used for grain characterization as a part of free volume analysis of a packing (Luchnikov et al., 2002) and for volumetric characterization of biomacromolecules in solution (Voloshin et al., 2014). Fractal analysis with Voronoi and statistical models for different shapes of contact surfaces leads to a better understanding of the influence of the fractal nature on the final microstructure and material properties (Baillis et al., 2017; Mitić et al., 2013). In this study, tessellation was used for characterizing the uniformity and homogeneity of the pore distribution.

Material testing methods allow the measurement of a defined material shape under loading in order to enable extrapolation to the behavior under exploitation. Experimental results give information about the macroscopic properties of an assembly, the average stress of the material (Tucker III and Moldenaers, 2002). Micromechanical examination gives insight into the mechanical behavior on the microscale, the stress distribution, and the impact of a microstructure on stress concentration. The micromechanical behavior of polymer blends is comparable to macroscopic results and may be used for evaluating the shear stress distribution in dependence on the pore diameters (Tomić et al., 2017). Strategies for the fabrication of porous materials based on polymer blends with highly controlled microstructure, which relates primarily to the diameters of the pores, have been reported in the literature (Wang et al., 2014). These studies leave space for a new strategy for controlling the mechanical properties of a material/adhesive by manipulation of the porosity by changing the chemical composition.

The structure of the material examined using the cross section visualization by the means of a scanning electron microscope gives the image of a microstructure where the pores can be visualized. The obtained images can be analyzed using image analysis tools in order to extract the exact positions of the pores in the structure and to characterize their morphological parameters, as well as the overall porosity of the material. There are several ways to obtain such information and Python scripting was proposed as an efficient way to transpose the obtained structural characteristics to the structure that could be representative of the actual structure a material for further simulation. Data for the construction of a characteristic structure that is then imported into a program that calculates the stress and strain distribution in a material under shear stress conditions (Pegg and Gill, 2016). The stress distribution in a porous structure can be calculated using the finite element method and there is a number of software available to perform this analysis. In the present research, SimuliaAbaqus software that enabled the evaluation of the stress and strain distribution corresponding to the observed structure was used. Numerical analysis enabled the determination of the stress concentration in a polymer network, changes in shear stress and modulus with changes in the diameter of the pores and porosity. Improvement of mechanical properties by modification with graft polymerization was confirmed by increased maximal shear stress of a material (Tomić et al., 2017).

The aim of this study was to evaluate the critical parameters of porous polymer blends EVA/PMMA using graphical, statistical and numerical methods, and to correlate them with the experimental mechanical behavior. The results of this analysis are crucial in the design of the structure of a material and its processing.

Fig. 1. Connected optical fibers with an adhesive prepared for tensile test (Tomić et al., 2017).

2. Experimental

2.1. Materials

Ethylene–vinyl acetate (EVA) copolymer (Elvax 410, 18% VA, DuPont, USA), monomer MMA (M55909, Sigma Aldrich) and PMMA homopolymer (Acryrex® CM-205, $\bar{M}_w$ = 90,400 g/mol, Chi Mei Corporation, Taiwan) were used in this work for the preparation of the polymer blends based on EVA/PMMA. Toluene (Lachemaas, Czech Republic, min. 99.0%) and acetone (Zorka Pharma Šabac, min. 99.5%) were used as solvents. Methyl ethyl ketone peroxide (MEKP) (Boyteroks A, BoytekRecineBoyaveKimya San Tic, As, Catalysts & Initiators), potassium persulfate and sodium metabisulfate (Sigma–Aldrich Chemie GmbH, Steinheim, p.a), were used as received as initiators. Optical fiber produced by DrakaCableteq, USA was used for polymer blend deposition and the testing of the micromechanical properties.

2.1.1. Preparation of EVA/PMMA copolymer blends

The polymer blends were prepared according to the literature (Tomić et al., 2017).

The first material, a physical polymer blend EVA/PMMA was obtained by mixing 5.00 g of PMMA and 5.00 g of EVA in 46.2 cm^3 in toluene for 8 h at 60 °C on a mechanical stirrer.

The second material, a modified EVA/PMMA blend with EVA-*g*-PMMA (raw EVA-*g*-PMMA) was produced in an *in-situ* free radical graft polymerization by dissolving 10.02 g EVA (25.40 wt.%) in 30.7 cm^3 MMA (71.75 wt.%), and then 0.14 g potassium persulfate (0.37 wt.%), 0.12 g sodium metabisulfite (0.29 wt.%) and 0.92 cm^3 MEKP (2.68 wt.%) were added and the mixture was heated for 3 h at 70 °C in a sealed container under atmospheric conditions. The obtained graft copolymer was dissolved in toluene to obtain a 20 wt.% solution, which was then used as an adhesive for the optical fibers.

2.2. Application of a coating on the surface of optical fibers

The optical fibers were coated using 20 wt.% solutions of the prepared polymer blends in a specially designed apparatus at 60 °C, as previously described in the literature (Milutinović-Nikolić et al., 2002). The nozzle could be easily changed in order to control the thickness of the coating. The thickness could also be controlled by optimizing the speed of fiber drawing. The radial velocity of rotation of the spinner was ω = 300 rpm and the axial speed was ν = 1.5 mm/s (Tomić et al., 2016).

2.3. Material characterization methods

2.3.2. SEM analysis of a polymer blends microstructure

Precise cross-sections of the samples, obtained using a sharp medical blade, were examined after deposition of a thin gold layer on the surface of the samples using a Mira3 Tescan field emission scanning electron microscope (FE-SEM), operated at 20 keV.

2.3.3. Image analysis for the determination of the geometrical parameters of the optical fiber and polymer blends

Using software Image-Pro Plus6.0 (Media Cybernetics) allowed the

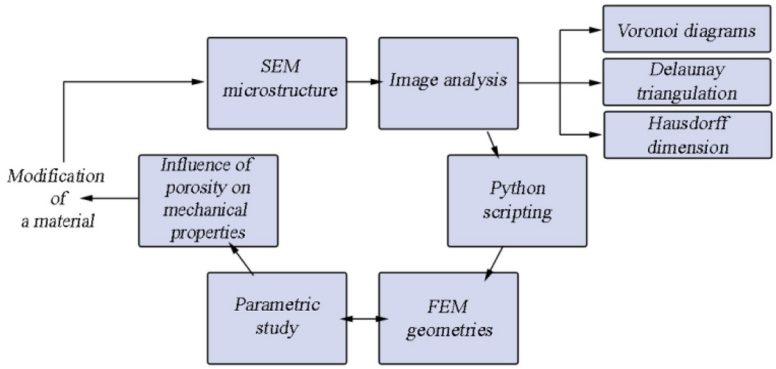

Fig. 2. The use of statistical and numerical analysis in the design of the microstructure of materials.

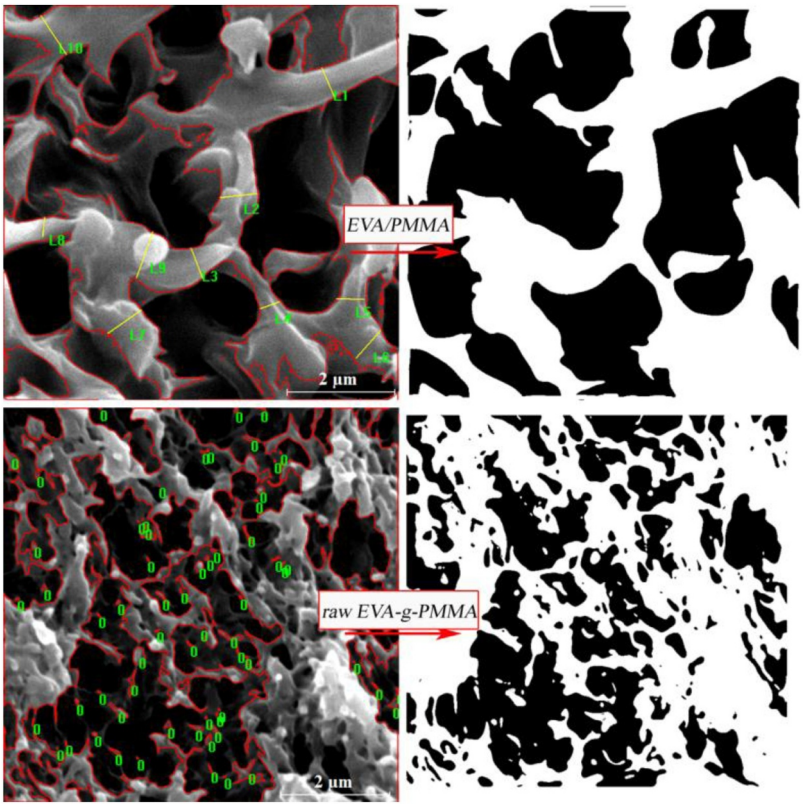

Fig. 3. Binary images (‘mask’) made by Image ProPlus based on SEM image that was used for image analysis.

statistical data of the diameters, spacing and porosity of the obtained polymer blends to be obtained. "Mask" made as a binary image of the processed SEM microstructure was used for obtaining parts for numerical analysis and further statistical examination.

2.3.4. Hausdorff dimension (DH_f)

Hausdorff dimension (DH_f) was used for assessing the information about the complexity of the porous network of a material that is related to the size and amount of pores. The calculation of the Hausdorff dimension was realized in Matlab7.12(r2011a) software on binary images, which were obtained by processing of microstructure on SEM images based on the grayscale level. The aim was to establish a calibration curve that predicts the pore diameter, which is appropriate for representation of the actual microstructure, *i.e.*, the polymer network.

2.3.5. Voronoi and Delaunay tessellation

Voronoi diagrams and Delaunay triangulation were used for characterizing the uniformity and homogeneity of the pore distribution in polymer blend and the distribution of the distances between the centers of the pores. The coordinates of the pore centers were obtained by image analysis in Image ProPlus 6.0 and processed in Octave 4.0.3 software.

2.3.6. Python scripting for Abaqus CAE

Python scripts were used for generating the geometry of parts for FEM simulation. Scripts were obtained by processing the coordinates of the pore contours by the Ramer–Douglas–Peucker algorithm (RDP) of a binary "mask" image, as well as for creation of the geometry for the "mirrored" part of a physical polymer blend.

Furthermore, Python scripts enabled a parametric study of the influence of diameter and porosity on the mechanical properties of porous polymer blends with established geometries having spherical shaped pores. Numerical simulation of the real microstructure part enabled quantification of the bulges of material that lower the porosity but will not participate in stress bearing.

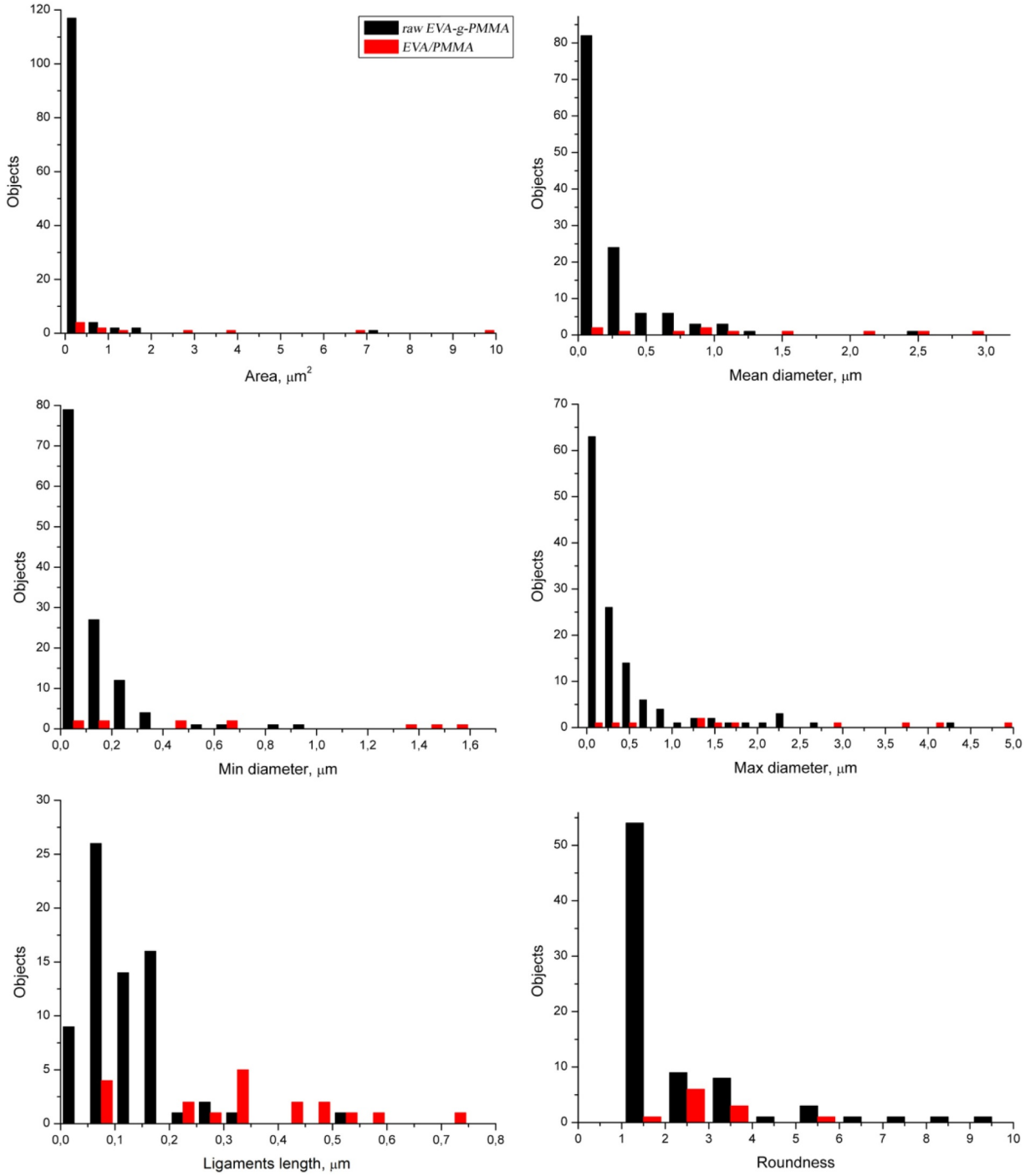

Fig. 4. Histogram of pore area, mean, minimal and maximal diameter, ligaments length and roundness.

2.3.7. Universal mechanical testing machine

Mechanical properties of polymer blends were investigated by a tension test adapted to the adhesion measurement using a Shimadzu AG-X plus tensile testing machine (100 N testing head). The optical fibers were 5 cm long where 1 cm of fiber was not connected with the other so it could be attached to the device, as shown in Fig. 1. The adhered section was 4 cm long. The deformation speed was 1 mm/min at ambient temperature. Three replicas of each measurement were made.

3. Results and discussion

3.1. Pore characterization with the aim of determining the critical parameters

When porous materials are obtained, the most frequent parameter used for describing porosity is the void content, pore diameter, area, fractal dimension, roundness, etc. (Berrezueta et al., 2015; Hyväluoma et al., 2017; Le et al., 2017; Liu and Ostadhassan, 2017; Zambrano et al., 2017). A recent study presented the difference in mechanical properties of porous EVA/PMMA polymer blends when the void content of two porous materials were very similar but they differed in their pore

Table 1
Descriptive statistical data provided by OriginPro 9.0 statistic tools in the analysis of the porosity parameters (area, pore diameters, critical ligament thickness and roundness) obtained by image analysis for porous polymer blends.

Porosity parameters	Area (μm^2)		Mean diameter (μm)		Max. diameter (μm)		Min.diameter (μm)		Critical ligaments thickness		Roundness	
Statistics	gb[a]	pb[a]	gb	pb	gb	pb	gb	pb	gb	pb	gb	pb
Objects	126	11	126	11	126	11	126	11	70	19	80	11
Mean	0.17	2.30	0.26	1.17	0.43	2.02	0.12	0.64	0.12	0.33	2.45	2.87
SD[b]	0.69	3.17	0.33	0.96	0.64	1.62	0.14	0.57	0.08	0.18	2.69	1.19
Variance	0.47	10.0	0.11	0.92	0.41	2.63	0.02	0.32	0.01	0.03	7.22	1.41
Sum	21.9	25.3	32.3	12.9	54.2	22.2	15.5	6.99	8.43	6.33	196.1	31.6
Skewness	8.41	1.62	3.50	0.79	3.19	0.64	3.56	0.77	2.64	0.19	4.49	1.81
Kurtosis	81.3	1.90	17.4	–0.49	12.6	–0.99	15.7	–0.95	11.3	–0.15	25.9	3.68
Minimum	0.01	0.01	0.03	0.10	0.04	0.17	0.02	0.04	0.04	0.06	1.00	1.80
Median	0.02	0.63	0.14	0.82	0.20	1.44	0.08	0.50	0.10	0.34	1.56	2.74
Maximum	7.03	9.62	2.50	2.99	4.31	4.85	0.93	1.59	0.55	0.73	20.5	5.86

[a] gb – raw EVA-*g*-PMMA; pb – EVA/PMMA;
[b] SD – standard deviation; variance – the ratio of the standard deviation to the mean; *skewness* – measures the degree of asymmetry of a distribution; *kurtosis* – depicts the degree of peakedness of a distribution; *min, median, max* – parameters of the range. (The *median* is the value separating the higher half of a data sample, or a probability distribution, from the lower half.)

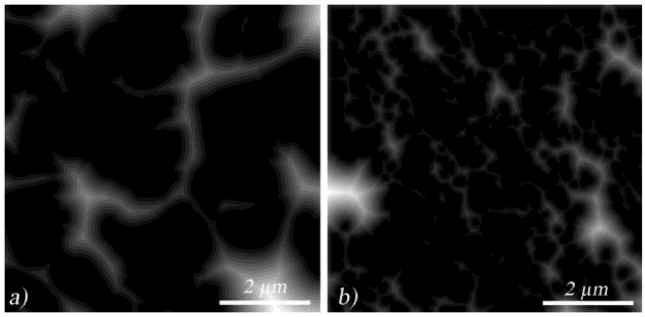

Fig. 5. Euclidean distance map of bitmap images used in image analysis based on SEM images (Fig. 3).

diameter (Tomić et al., 2017). The focus of the present paper was to ascertain the impact of critical parameters that are not related exclusively to the pore diameter but also their shape complexity. The complex pores were related to the shape of spherical pores by the Hausdorff dimension. The distribution of pores in the material was characterized by Voronoi and Delaunay triangulation. The main idea of pore characterization is presented in Fig. 2.

Image ProPlus software enabled the extraction of light and dark parts of the picture, *i.e.*, the part of the polymer blend that is in contact with the surface of the optical fiber and the empty space or pores (Dimitrijevic et al., 2012). The mask that was obtained and used in the characterization is shown on the right side of Fig. 3. The histogram of critical parameters defining pores and pore distribution showed the main differences between the physical polymers blend EVA/PMMA and raw EVA-*g*-PMMA graft copolymer blend (Fig. 4). The critical ligament thickness was measured *via* image analysis selecting only critical/minimal values.

Mean values of studied parameters are far lower for raw EVA-*g*-PMMA including a large amount of objects than for physical blend EVA/PMMA. This result is a consequence of achieved compatibilization with employed graft polymer EVA-*g*-PMMA. Pores of EVA/PMMA had an area 13 times larger; 4.5 times larger mean diameter; 2.75 times thicker ligaments; 1.2 times larger roundness than pores of raw EVA-*g*-PMMA. High dimension of pores leads to a weaker structure and intense stress concentration. Thicker ligaments stabilize the applied load to the weak structure of EVA/PMMA. The most critical parameter in a case of raw EVA-*g*-PMMA was the thickness of the ligaments, where the pore distribution ensured homogeneity of the sample and effective stress distribution. The roundness of the pores of raw EVA-*g*-PMMA, having values near 1, suggests that these pores are closer to spherical than those of EVA/PMMA. Analyzing the distribution of the parameters, the best fitting of data describing the pores of raw-EVA-*g*-PMMA was found in a log-normal distribution, while the polymer blend EVA/PMMA exhibit a nondefined type of distribution, since the data were mostly equally distributed along the *x*-axis.

To obtain more detailed information about the distribution of porosity parameters, descriptive statistics was performed on data extracted using the image analysis tools (Fig. 4). Statistical analysis was realized using the standard statistics tools available in OriginPro 9.0 and the data are presented in Table 1. The high skewness of the distribution for raw EVA-*g*-PMMA showed concentration of the pore parameters around the mean value, which was represented also by a lower value of variance in relation to EVA/PMMA. The extremely high kurtosis values of the compatibilized polymer blend (raw EVA-*g*-PMMA) indicated that the mean value of the pore parameters was representative in the characterization of pores, having a lower mean value of dissipation. Negative values of kurtosis were obtained for EVA/PMMA due to the large scattering of values, suggesting the amounts of large and small pores were similar. Mean values for pore diameters were used in numerical simulation of the stress distribution in order to evaluate their influence. Image analysis determined the porosity on SEM images that was used for FEM part generating, with values: EVA/PMMA – 52.4%, raw EVA-*g*-PMMA – 40.5%.

An Euclidean distance map (EDM) filter was used in the SEM image analysis (Fig. 3) using Image ProPlus software in order to obtain the polymer network of the material that represents the line connecting the centers of mass along the material (Fig. 5). Such a presentation of the SEM images enabled the main load bearing centers and also the weak points where the white network fades to be located. Fig. 5 shows that EVA/PMMA had simultaneously concentrated regions of bearing and weak regions with a weak network of the material. The emphasized thick ligaments connect these regions in a far simpler way than in the case of raw EVA-*g*-PMMA. Multiple branches of the centers of mass in the complex raw EVA-*g*-PMMA network stabilize stress in more directions, allowing better mechanical performance of the raw EVA-*g*-PMMA material.

When the SEM images of cross-sections of the polymer blends were analyzed, bulges could be noticed that could play the role in decreasing the porosity but they make no contribution to bearing the stress. The Hausdorff dimension (DH_f) was determined for regular shaped pores with diameter corresponding to the minimal, mean and maximal diameter for EVA/PMMA polymer blend and that region was found to be convenient for determining the diameter that describes irregular pores related to DH_f. Predictions of regular pore diameters that describe the irregular pores by using the Hausdorff dimension relating to the complexity of the porous polymer blend are presented in Fig. 6.When comparing the binary images representing pore detection for polymer

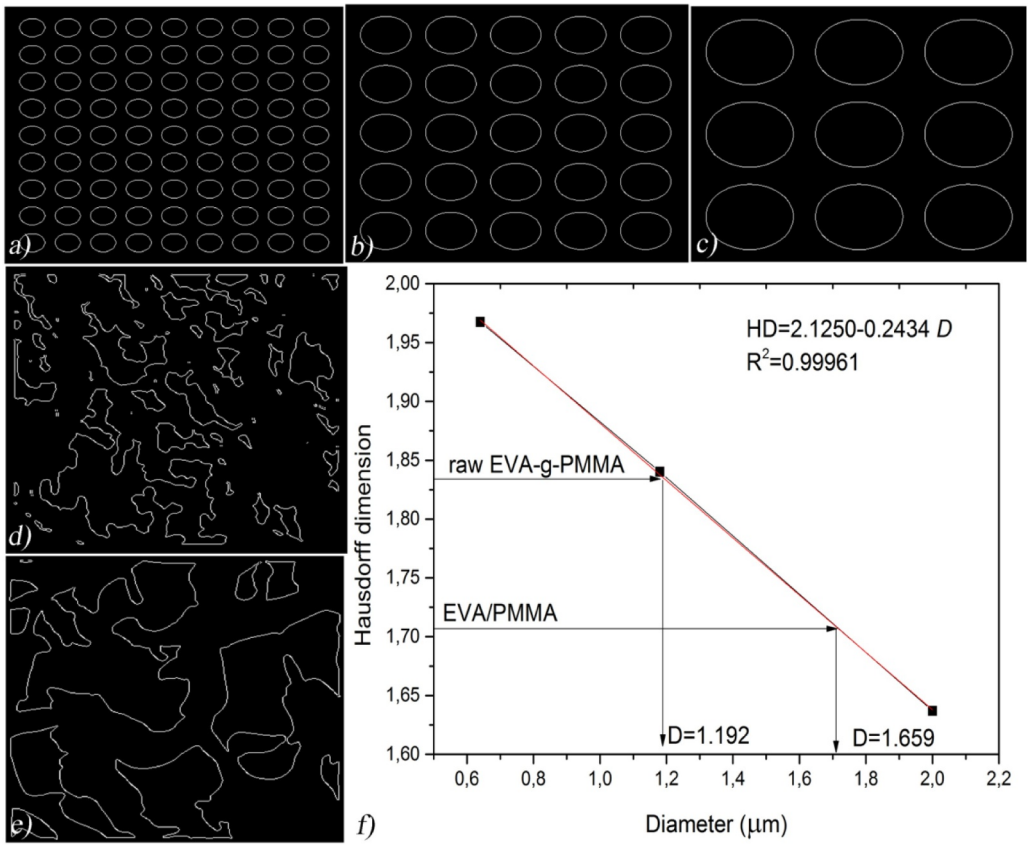

Fig. 6. Regular shapes of the pores with diameters corresponding to the: a) D_{min}, b) D_{mean}, c) D_{max}, with the microstructures of the polymer blends: d) raw EVA-*g*-PMMA, e) EVA/PMMA, and derived dependence f) Hausdorff dimension *versus* diameter.

blends (Fig. 6d and e), it could be observed that the images are characterized by high quality of the detected pores (Stach et al., 2014). The lower DH_f value for EVA/PMMA (1.7206) than for raw EVA-*g*-PMMA (1.8353) suggests that EVA/PMMA has a microstructure with a smaller number of pores with larger diameters, as seen by statistical analysis (Fig. 6). The higher DH_f value for raw EVA-*g*-PMMA may indicate possible superior mechanical properties compared to the EVA/PMMA polymer blend with a microstructure that enables effective load distribution and stabilization. The complexity of networks of raw EVA-*g*-PMMA and EVA/PMMA materials may be related to the network obtained by spherical pores of 1.192 and 1.659 μm, respectively. The multi-pore network of smaller diameters makes the web denser that allows the material to better stabilize and distribute the load.

The employed Voronoi tessellation estimated the ratio of the Voronoi regions that correspond to the pore centers of the polymer blend, the pore uniformity and characterization of pore distribution for both materials (Fig. 7). The Voronoi network emphasized the higher number of small pores with a better distribution in the raw EVA-*g*-PMMA polymer blend and the advantage of microstructure regularity. The network density was reflected in the number of traced pores that are presented as the number of the Voronoi area on the statistical histogram in Fig. 7. The scripts for Octave software excluded marginal Voronoi regions that can significantly increase the average value of the Voronoi area that will not be representative. In this manner, the number of regions of EVA/PMMA was decreased and it was not possible to calculate the kurtosis and the skewness for the physical blend, while raw EVA-*g*-PMMA showed high values for kurtosis and skewness representing good pore uniformity over the cross-section (Table 2). The SD and variance suggested that the compatibilized polymer blend, raw EVA-*g*-PMMA, had a higher uniformity of the porous microstructure than that of the uncompatibilized EVA/PMMA polymer blend. The percentage ratio of the mean value of pore area and mean Voronoi area represents the occupation of the Voronoi region with a pore. These ratios for the mean values are EVA/PMMA – 30.3% and raw EVA-*g*-PMMA – 18.9%; and for the median values: EVA/PMMA – 8.3% and raw EVA-*g*-PMMA – 3.4%. The mean value of the two remaining Voronoi areas showed that the value of EVA/PMMA was more than 8 times higher than that of raw EVA-*g*-PMMA.

Studied pores of the polymer blends have a very complex shape with an indented outline that penetrates in more than one Voronoi region, so this represents a simplified method of the determination of the pore uniformity and the tool for comparing the pore distribution.

The Delaunay triangulation is useful in the calculation of distances between selected objects. Image ProPlus was used for obtaining the coordinates of the pore centers that were implemented into the script for Octave software (Fig. 8). The descriptive statistics parameters of the distribution of the pore distances showed higher symmetry and kurtosis for raw EVA-*g*-PMMA than for the physical blend EVA/PMMA (Table 3). The variance for raw EVA-*g*-PMMA showed less dissipation of distances than that for EVA/PMMA. The lower the variance is, the lower is the dissipation and the better is the uniformity of the microstructure, which ensures better mechanical properties. Comparing mean values for pore diameter (Table 1) and center distance (Table 3), it can be calculated for EVA/PMMA polymer blend that the line connecting two pore centers crosses along 40.3% of their length through a pore, while in raw EVA-*g*-PMMA crossing through a pore was lowered to 25.2% of the distance. Such results indicate the presence of small pores with thin ligaments for raw EVA-*g*-PMMA (mean value 0.77 μm) and larger pores with thicker ligaments for EVA/PMMA (mean value 1.73 μm).

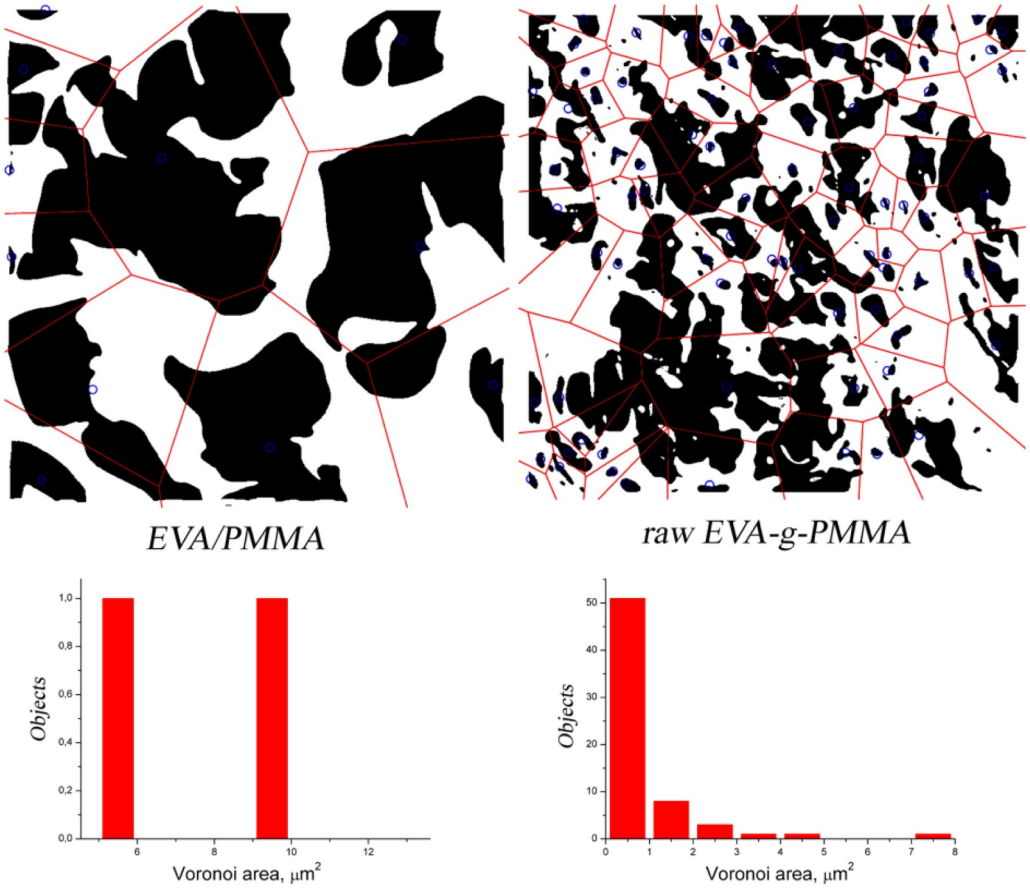

Fig. 7. Voronoi diagrams and histograms of the Voronoi area distribution for polymer blends EVA/PMMA and raw EVA-*g*-PMMA.

Table 2
Descriptive statistic parameters of Voronoi area distribution (μm^2).

	Object analyzed	Mean	SD[b]	Variance	Sum	Skewness	Kurtosis	Min	Median	Max
pb[a]	2	7.58	2.67	7.15	15.15	–	–	5.69	7.58	9.47
gb[a]	65	0.90	1.10	1.20	58.37	3.73	16.73	0.12	0.59	7.05

[a] gb – raw EVA-*g*-PMMA; pb – EVA/PMMA;
[b] SD – standard deviation; *variance* – the ratio of the standard deviation to the mean; *skewness* – measures the degree of asymmetry of a distribution; *kurtosis* – depicts the degree of peakedness of a distribution; *min, median, max* – parameters of the range. (The *median* is the value separating the higher half of a data sample, or a probability distribution, from the lower half.)

3.2. Finite element method and Python scripting for evaluating the influence of critical parameters

Finite element models of the polymer blends used as adhesives, the physical polymer blend (EVA/PMMA) and the graft modified polymer blend (raw EVA-*g*-PMMA), were established. The main differences between the materials were found in mechanical properties and microstructure (porosity parameters). A scheme of the analyzed models of adhesive segment is presented in Fig. 9, according to the experimental setup shown in Fig. 1. The adhesive segment in numerical analysis was exposed to shear loading. In addition, the set of boundary conditions are presented in Fig. 9, where the left side of the adhesive cell was constrained and a displacement was prescribed to the right side.

The models with the use of SEM microphotographs corresponding to the graft polymer blend raw EVA-*g*-PMMA and physical polymer blend EVA/PMMA are shown in Fig. 10. The geometries were formed using Python scripts with coordinates obtained from SEM microphotographs by image analysis and meshed using CPE4 finite elements in Abaqus-4-node bilinear plane strain quadrilateral elements with full integration. Simulation was performed in a static general step, bearing in mind that the experiment was conducted under quasi-static conditions. Elastic–-plastic material behavior, based on the tensile properties of the material under static conditions, was used as the model of the material. Strain rate dependence was not taken into account in the model, since the experiment was performed at a low strain rate.

Microstructure cells from Fig. 10 were examined in order to obtain the differences in mechanical behavior and the critical points of stress distribution of the porous polymer blends.

Further examination was performed using Python scripting for scale-up of the geometry of EVA/PMMA using the rotation/mirror image procedure shown in Fig. 11. The scale-up process was realized with the aim of investigating the influence of the complexity of examined microstructure in a case of uniform microstructure along the whole material. The scale-up process did not lead to significant differences in the results.

After consideration of the different microstructure of the two polymer blends represented by the models in Fig. 10, the differences in mechanical properties were considered. The contribution to the improved mechanical properties of raw EVA-*g*-PMMA was mainly due to the higher PMMA content, but also due to the different fabrication

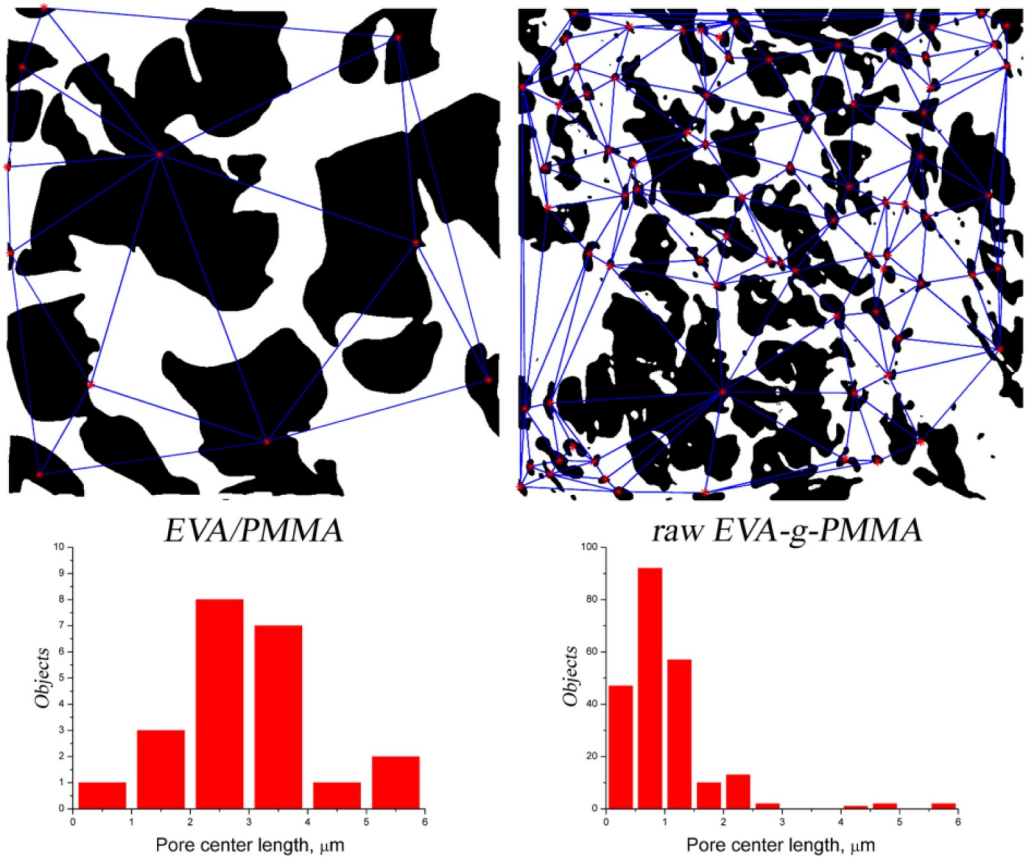

Fig. 8. Delaunay triangulations used for measuring the distance between the pore centers.

Table 3
Descriptive statistic parameters for the distribution of the Delaunay distance (μm).

	Object analyzed	Mean	SD[b]	Variance	Sum	Skewness	Kurtosis	Min	Median	Max
pb[a]	22	2.90	1.15	1.31	63.91	0.22	–0.36	0.91	2.82	5.09
gb[a]	226	1.03	0.80	0.64	232.63	3.11	13.50	0.16	0.89	5.78

[a] gb – raw EVA-*g*-PMMA; pb – EVA/PMMA;
[b] SD – standard deviation; *variance* – the ratio of the standard deviation to the mean; *skewness* – measures the degree of asymmetry of a distribution; *kurtosis* – depicts the degree of peakedness of a distribution; *min, median, max* – parameters of the range. (The *median* is the value separating the higher half of a data sample, or a probability distribution, from the lower half.)

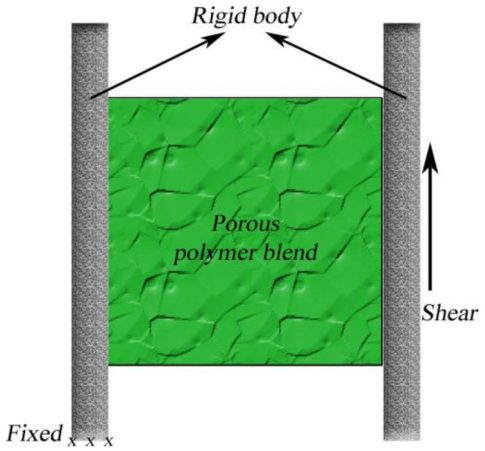

Fig. 9. The adhesive cell used in the numerical analysis with boundary conditions.

procedure. *In situ* graft compatibilization led to improved interfacial adhesion of the polymer constituents. The prediction of mechanical properties was obtained considering the mixture rules for polymer blends proposed by the Equivalent Box Model (EBM) with equations for elastic modulus (E_b) and yield strength (S_b) (Kolařk, 1998):

$$E_p = (E_1\nu_{1p} + E_1\nu_{2p})/\nu_p \tag{10}$$

$$E_s = \nu_p/[(\nu_{1s}/E_1 + \nu_{2s}/E_2)] \tag{11}$$

$$E_b = E_p\nu_p + E_s\nu_s \tag{12}$$

$$S_b = (S_1\nu_{1p} + S_2\nu_{1s}) + AS_1\nu_s S_b = (S_1\nu_{1p} + S_2\nu_{1s}) + AS_1\nu_s \tag{13}$$

where E_p and E_s are the moduli in the parallel and series branches of EBM. The volume fractions of each component ν_{ij} coupled in parallel (subscript j = p) or in series (subscript j = s) are interrelated as follows:

$$\nu_{1p} = [(\nu_1 - \nu_{1cr})/(\nu_1 - \nu_{1cr})]^{t_1};\ \ \nu_{2p} = [(\nu_2 - \nu_{2cr})/(\nu_2 - \nu_{2cr})]^{t_2}\nu_{2p} = [(\nu_2 - \nu_{2cr})/(\nu_2 - \nu_{2cr})]^{t_2} \tag{14}$$

$$\nu_p = \nu_{1p} + \nu_{2p};\ \ \nu_s = \nu_{1s} + \nu_{2s};\ \ \nu_1 = \nu_{1p} + \nu_{1s};\ \ \nu_2 = \nu_{2p} + \nu_{2s};\ \ \nu_1 + \nu_2 = \nu_p + \nu_s = 1\nu_1 + \nu_2 = \nu_p + \nu_s = 1 \tag{15}$$

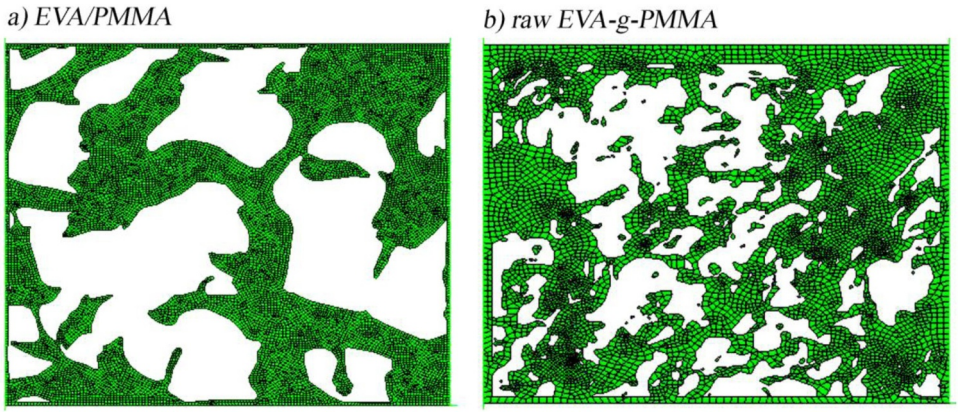

Fig. 10. Parts used in the FEM analysis representing a physical polymer blend EVA/PMMA and a modified polymer blend raw EVA-*g*-PMMA.

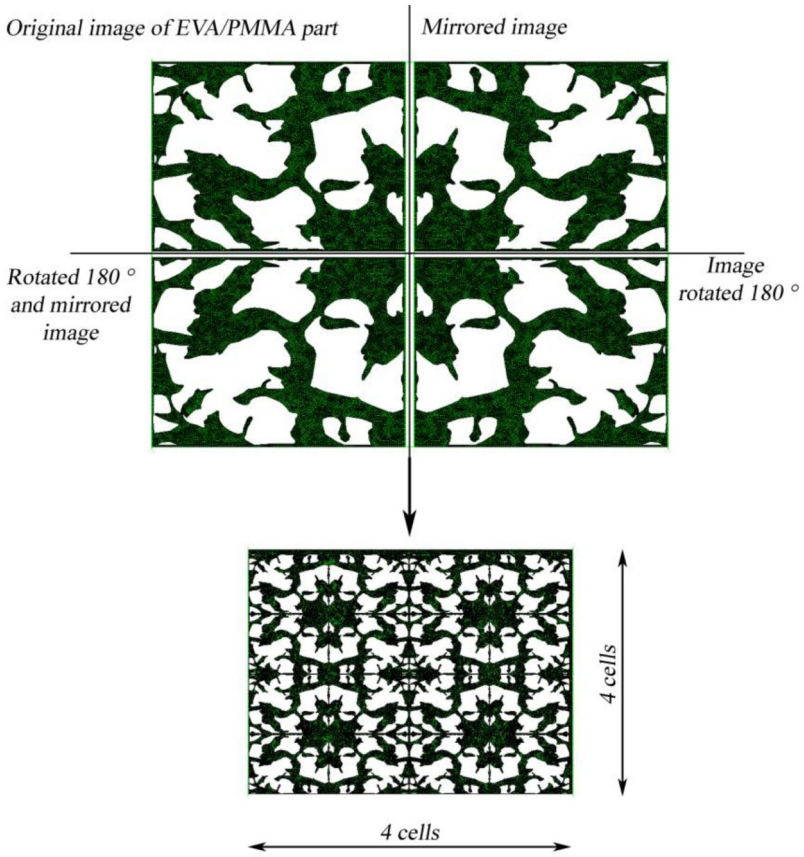

Fig. 11. Scale up of the microstructure of the physical polymer blend.

Table 4
Mechanical properties of the parent polymers and polymer blends used in EBM

	Modulus of elasticity (E)[a] (MPa)	Poisson ratio (ν)[a]	Yield strength (S) (MPa)
EVA	33	0.35	22[b]
PMMA	2000	0.35	98[c]
raw EVA-*g*-PMMA	1092	0.35	57
EVA/PMMA	443	0.35	25

[a] According to Duncan et al. (n.d.).
[b] According to Alothman, 2012.
[c] According to Zebarjad et al. (2011).

where $\nu_{cr} = 0.156$ and $t = 1.8$ are universal constants found in the literature (Klein et al., 1991). Subscript $i = 1$ denotes the first polymer component (EVA) and $i = 2$ for the second (PMMA); A is the extent of interfacial debonding having values between 0 and 1 and in this case will depend on the degree of compatibilization. Incompatibility of polymers causes low interfacial adhesion that enable complete debonding between the phases in a series ($A = 0$ in yield stress). Idealized compatibility is represented with strong interfacial adhesion that effectively transfers the stress between the polymer constituents without debonding ($A = 1$) (*Processing and Finishing of Polymeric Materials*, 2 Volume Set, 2011).

EVA/PMMA has very weak interactions due to the immiscibility of EVA and PMMA and hence, a low value for interfacial debonding was taken into an account: $A = 0.1$. *In situ* compatibilization was performed with the aim of improving miscibility, which was shown by the higher

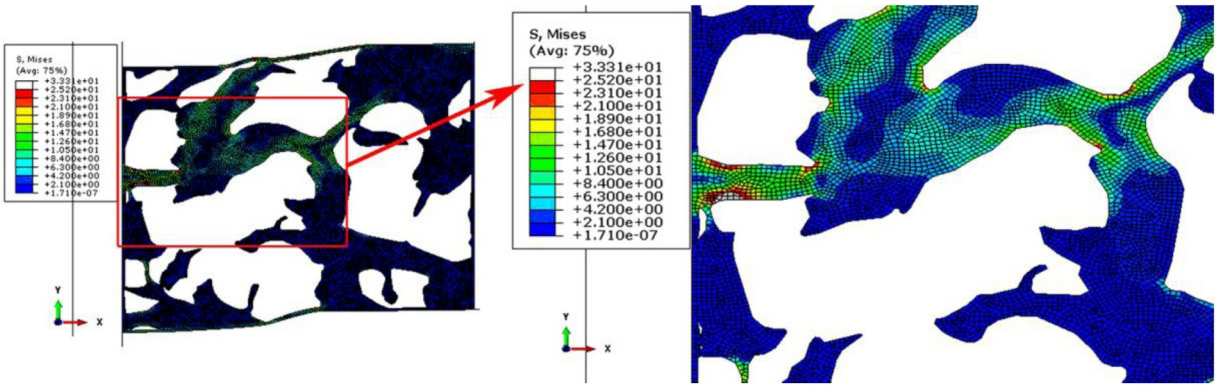

Fig. 12. Equivalent von Mises stress distribution in a realistic microstructure of the physical polymer blend EVA/PMMA.

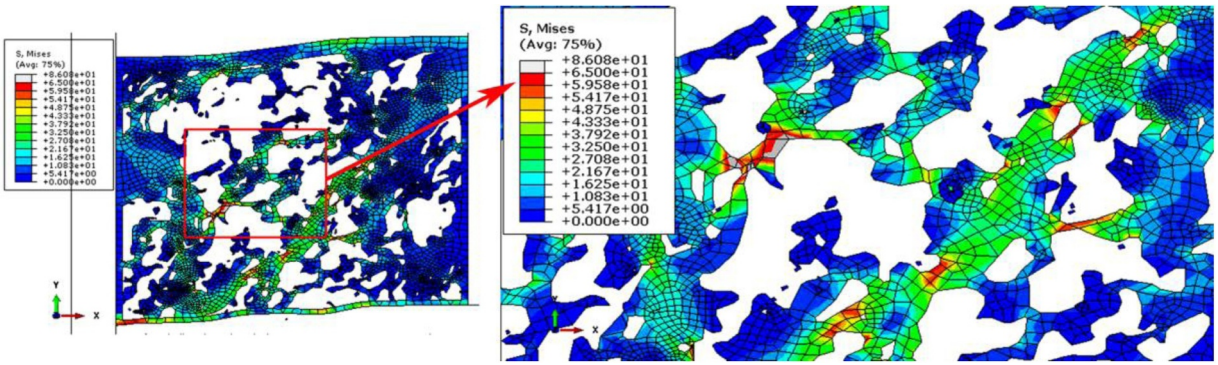

Fig. 13. Equivalent von Mises stress distribution in a realistic microstructure of the modified polymer blend raw EVA-*g*-PMMA.

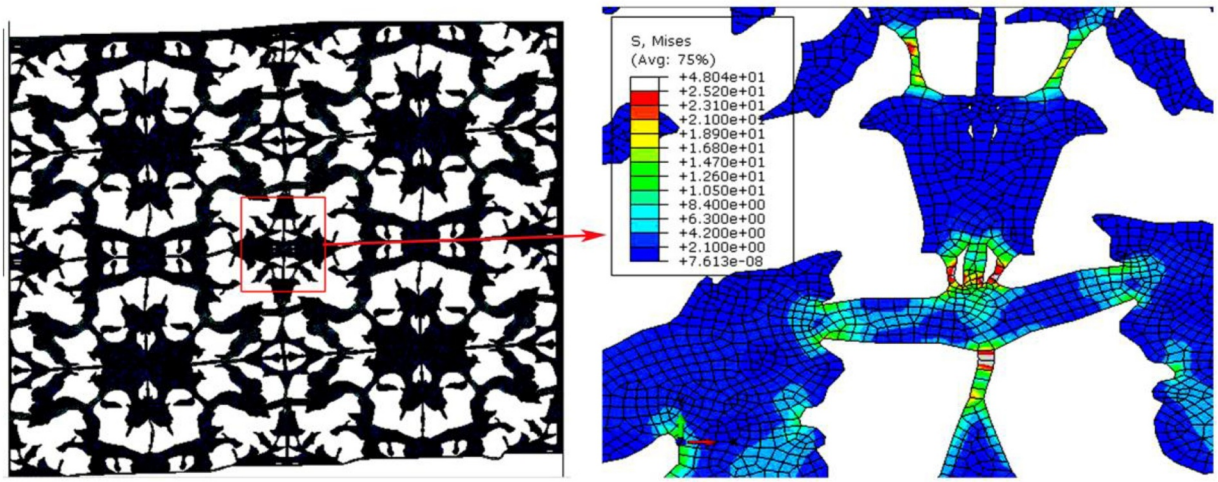

Fig. 14. Equivalent von Mises stress distribution in the scaled-up microstructure of the physical polymer blend EVA/PMMA.

tensile strength in experimental tests, and thus $A = 0.5$ was used in the prediction of yield strength for raw EVA-*g*-PMMA. The mechanical properties of the parent polymers (EVA and PMMA) used in determining the properties corresponding to the polymer blend (raw EVA-*g*-PMMA and EVA/PMMA) are presented in Table 4.

The mechanical properties obtained for EVA/PMMA were very similar to the ones for pure EVA. Infrared spectroscopy (FTIR analysis) showed that a blend with an EVA content of 50%, due to the immiscibility of polymers, exhibited a dominance of the EVA chemical structure (Tomić et al., 2017). Thus, a prediction of mechanical properties was assumed to be proper for finite element analysis. Based on the increased incompatibility of EVA and PMMA in a weight ratio 50/50, this polymer exhibits very weak interfacial adhesion between the polymer constituents, and therefore the influence of PMMA on mechanical properties was negligible.

The compatibilized polymer blend (raw EVA-*g*-PMMA) had a lower EVA content (approx. 25 wt. % of EVA and 75 wt. % of PMMA) the miscibility/compatibility was increased, which influenced the mechanical properties. A decrease in mechanical properties of EVA/PMMA polymer blends when compared to pure PMMA was in the ranges presented for PMMA/EVA blends with the PMMA content ≈80% (Poomalai et al., 2007).

Equivalent von Mises stress fields for all three models are shown in Figs. 12–14. The maximum values on these contours shown as red fields correspond to the calculated yield strength values of polymer blends Eqs. (10)–((15)). Figs. 12–14 show stress fields that indicate the

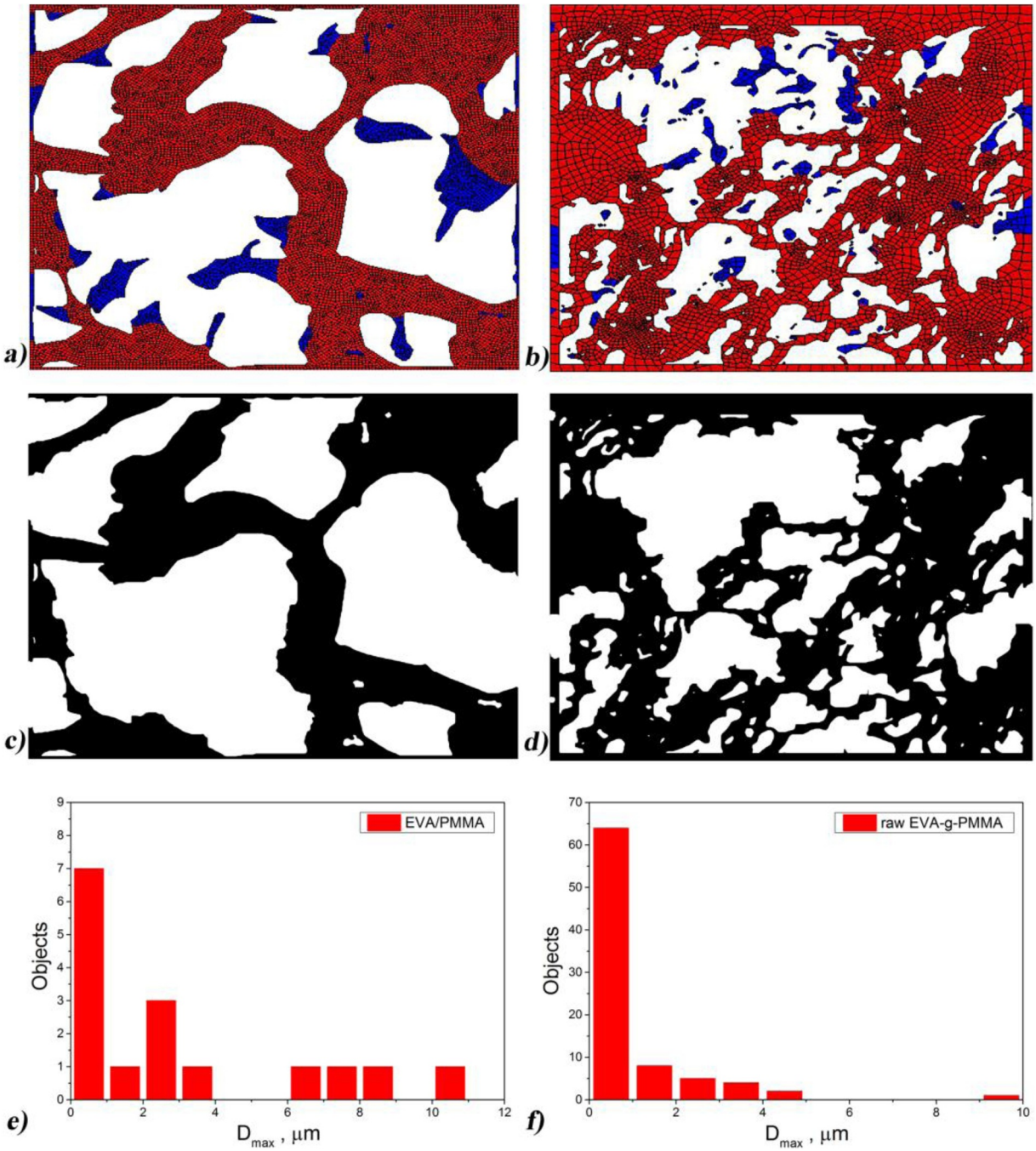

Fig. 15. Numerical models used for analyzing the stress distribution: a) EVA/PMMA, b) raw EVA-*g*-PMMA (red – bearing elements, blue – non-bearing); masks created in Image ProPlus by excluding elements that do not carry load: c) EVA/PMMA, d) raw EVA-*g*-PMMA; histograms representing the change in the porosity parameter (D_{max}) for: e) EVA/PMMA, f) raw EVA-*g*-PMMA.

Table 5
Statistical data from image analysis of the derived Fig. 16c and d, for EVA/PMMA and raw EVA-*g*-PMMA, respectively.

	Area (µm^2)	Max diameter (µm)	Min diameter (µm)	Mean diameter (µm)	Roundness	Fractal dimension
raw EVA-*g*-PMMA	0.95 (3.45)[a]	1.04 (1.39)	0.35 (0.41)	0.63 (0.79)	1.89 (0.94)	1.07 (0.03)
EVA/PMMA	7.08 (12.4)	2.98 (3.17)	1.35 (1.70)	1.93 (2.16)	1.90 (0.49)	1.06 (0.03)

[a] Values in parenthesis represent SD.

yielding occurred in thin ligaments between the voids. The larger voids in the EVA/PMMA polymer blend exhibited more significant deformation, i.e. shape change, and the yieldings were more pronounced. The modified polymer blend, raw EVA-*g*-PMMA, has a higher value of shear stress than the physical polymer blend EVA/PMMA. Scaled-up model of EVA/PMMA ('mirror' model, Fig. 14) emphasized stress concentration on thin ligaments. This model indicated the most critical points of possible material failure that were not been clearly shown on a single

Table 6
Descriptive statistics data of D_{max} (μm) of pores created by FEM.

	Objects analyzed	Mean	*SD*	Variance	Sum	Skewness	Kurtosis	Min	Median	Max
raw EVA-*g*-PMMA	84.00	1.04	1.39	1.95	87.14	3.37	15.46	0.12	0.54	9.41
EVA/PMMA	16.00	2.98	3.17	10.69	47.66	1.18	0.18	0.18	1.71	10.34

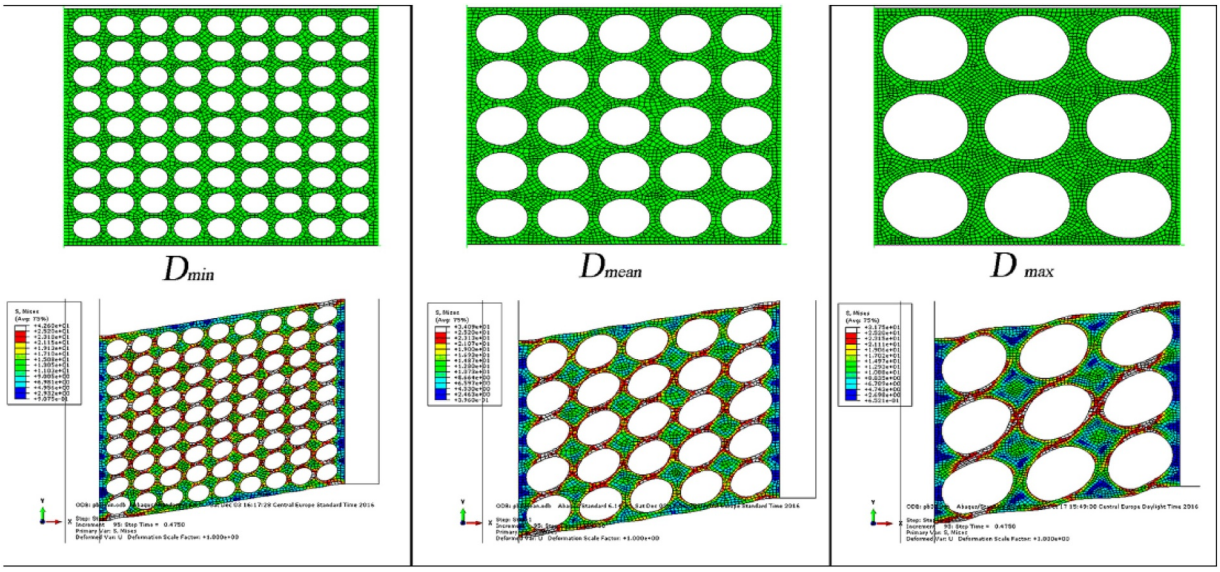

Fig. 16. Parts with spherical shape of pores used to determine the influence of pore diameter on the shear behavior of the physical EVA/PMMA polymer blend.

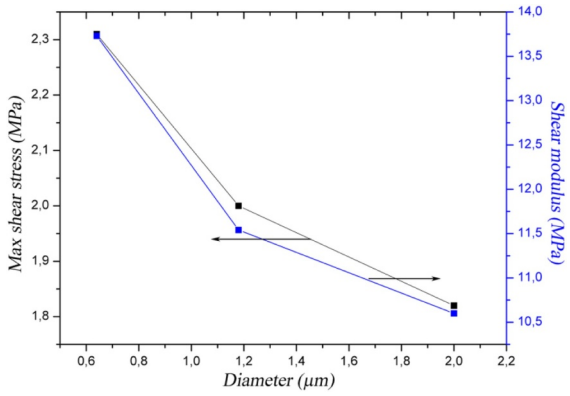

Fig. 17. Dependence of the shear stress/modulus on the pore diameter for the physical polymer blend EVA/PMMA.

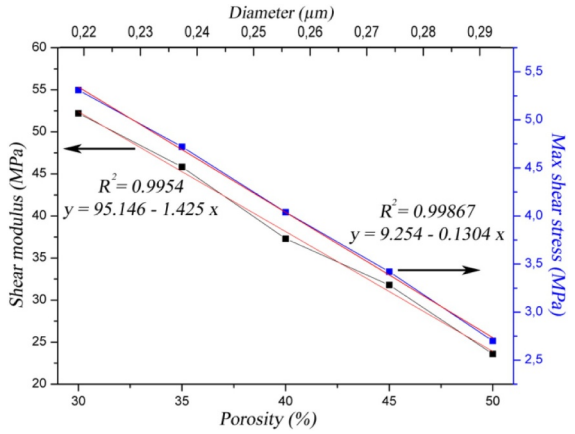

Fig. 18. Dependence of shear modulus/stress on the porosity of the physical polymer blend EVA/PMMA.

cell.

The physical polymer blend EVA/PMMA in numerical analysis showed the expected lower mechanical behavior than raw EVA-*g*-PMMA. The aim of comparing the numerical results of the established models was to gain insight into the differences in mechanical behavior of two analyzed polymer blends. From the present results of the numerical analysis, it could be concluded that the difference in mechanical behavior of the two examined adhesives was caused by both the mechanical properties (values of Young modulus and yield strength) and the real state of the microstructure (porosity, pore dimensions and distribution).

By analyzing the stress distribution of finite elements (Figs. 12 and 13) by setting the limit for stress bearing elements in display settings in Abaqus (1% yield stress), it was possible to gain insight into the non-bearing elements (blue regions) that should be excluded from the analysis of the porosity parameters (Fig. 15). The non-bearing regions were eliminated from the image and the image analysis was repeated. The increase in porosity for EVA/PMMA was higher (7.6%) than that for raw EVA-*g*-PMMA (1.3%) as a consequence of pores with larger diameters, and where the bulges were of large dimensions, which leads to a larger area of non-bearing elements. Masks from the image analysis (Fig. 15c and d) with bearing elements (red area from Fig. 15a and b, respectively) were analyzed, and the statistics data are presented in Table 5.

It can be noticed that all the analyzed parameters are higher when just the bearing elements were analyzed except for the roundness, which suggest that the shape of pores became closer to the shape of a sphere. Furthermore, the maximal diameter was investigated, and the distribution of the maximal diameters of the measured objects is presented in Fig. 15e and f. To quantify the distribution, descriptive statistics of the pores, D_{max}, are presented in Table 6. When the data obtained from Table 3 are compared with the date from Table 1, it could be concluded that the descriptive data for the maximal diameter of the

bearing elements (mean, min, max and median values) were more than two times higher than the microstructure with the non-bearing elements included. Only the standard deviation (SD) and the variance were lower since the roundness was closer to 1 (Table 5) and the dissipation of the data was lowered.

3.2.1. Parametric study of the influence of critical parameters on the mechanical properties using Python scripting in Abaqus CAE

The influence of the meshed parts used in the parametric study of the pore diameter on the mechanical properties for physical polymer blend EVA/PMMA is presented in Fig. 16. The mean values for D_{min}, D_{mean}, and D_{max} from Table 1, obtained from image analysis and with same porosity for all models, 55%, were used. Highlighted deformation with larger regions of yielding of EVA/PMMA material was present when the maximal diameter was used. Minimal diameter was able to stabilize the shear stress and to distribute stress evenly through the material structure.

The maximal values of the shear stress and shear modulus for models of each diameter are presented in Fig. 17. Drastically decreased mechanical properties were noticed when the diameter was increased. The obtained results indicated that the diameter, shape and the distribution of the pores are of great importance in establishing a proper estimation of the mechanical properties.

The main parameter that determines the mechanical behavior of porous materials is the porosity itself. This parametric study is based on the examination of the influence of porosity on the mechanical properties of the EVA/PMMA polymer blend (Fig. 18). The diameter of the pores was set so the distribution and number of pores were constant, and the porosity was changed in the range 30–50% (with 5% intervals). A linear dependence was observed, and with the increasing porosity by 10% (from 30% to 40%), the maximal shear stress that the material could withstand drops by 22%. Such a fact is important because of the existence of bulges that do not participate in stress bearing (Figs. 12–14) and additionally lower the mechanical performance of the polymer blend.

4. Conclusions

This study was focused on establishing the correlation between the parameters describing the porosity and their influence on mechanical properties of materials based on EVA/PMMA polymer blends. The modification by graft compatibilization in raw EVA-*g*-PMMA polymer blend improved the distribution of pores, lowered the pore dimension, and thus a better uniformity of the polymer blend was achieved. Hausdorff dimension (DH_f) analysis represents a new approach for detailed examination of the microstructure of porous materials, and furthermore, the prediction of mechanical properties. Based on this analysis, a procedure for selecting a model with regular pore shape and distribution based on the actual (irregular) porous microstructure is proposed. The irregular shape of the pores of EVA/PMMA polymer blends may be represented by regular-shaped pores with a diameter of 1.659 μm, and the modified polymer blend raw EVA-*g*-PMMA with pores of 1.192 μm in diameter. Characterization of SEM images by image analysis enabled detailed description of pore dimensions and porosity of the polymer blends, and gave the coordinates of pore centers, which were used in the Voronoi/Delaunay characterization of the preferable graphical display of pore distribution. Python scripts for SimuliaAbaqus were used for establishing the geometry of the models for numerical simulation based on the realistic microstructure of polymer blends, whereby the influence of non-bearing material (bulges), thin ligaments and the distribution of the pores was shown. The results from numerical analysis of the realistic microstructures indicated that the experimental results were the consequence of the material properties and the porosity parameters. Python scripts were also used in a parametric study, where the shear properties (modulus and strength) decreased drastically with increasing pore diameter and a linear dependence was obtained for shear stress/modulus and porosity. A decrease of 22% of maximal shear stress when porosity increased by 10% suggested the importance of bulging of the material that played the role of decreasing the porosity of non-bearing material.

Acknowledgements

This research was financed by the Ministry of Education, Science and Technological Development of the Republic of Serbia as a part of the projects TR34011, ON174004 and III45019.

References

Processing and Finishing of Polymeric Materials 2 Volume Set John Wiley & Sons, Inc.
Alothman, O.Y., 2012. Processing and characterization of high density polyethylene/ethylene vinyl acetate blends with different VA contents. Adv. Mater. Sci. Eng. 2012, 1–10. https://doi.org/10.1155/2012/635693.
Baillis, D., Conquard, R., Cunsolo, S., 2017. Effective conductivity of Voronoi's closed- and open-cell foams: analytical laws and numerical results, J. Mater. Sci., 52, 11146–11167. doi:10.1007/s10853-017-1226-z.
Berrezueta, E., González-Menéndez, L., Ordóñez-Casado, B., Olaya, P., 2015. Pore network quantification of sandstones under experimental CO_2 injection using image analysis. Comput. Geosci. 77, 97–110. https://doi.org/10.1016/j.cageo.2015.01.005.
Dimitrijevic, M., Veljovic, D., Posarac-Markovic, M., Jancic-Heinemann, R., Volkov-Husovic, T., Zrilic, M., 2012. Mechanical properties correlation to processing parameters for advanced alumina based refractories. Sci. Sinter. 44, 25–33. https://doi.org/10.2298/SOS1201025D.
Dimitrova, T., La Mantia, F., Pilati, F., Toselli, M., Valenza, A., Visco, A., 2000. On the compatibilization of PET/HDPE blends through a new class of copolyesters. Polymer (Guildf.) 41, 4817–4824. https://doi.org/10.1016/S0032-3861(99)00709-0.
Duncan, B., Mera, R., Leatherdale, D., Taylor M., M.R., 2005. Techniques for characterizing the wetting, coating and spreading of adhesives on surfaces. National Physical Laboratory, London, UK.
Hyväluoma, J., Kulju, S., Hannula, M., Wikberg, H., Källi, A., Rasa, K., 2017. Quantitative characterization of pore structure of several biochars with 3D imaging. Environ. Sci. Pollut. Res. https://doi.org/10.1007/s11356-017-8823-x.
Jiao, K., Yao, S., Liu, C., Gao, Y., Wu, H., Li, M., Tang, Z., 2014. The characterization and quantitative analysis of nanopores in unconventional gas reservoirs utilizing FESEM–FIB and image processing: an example from the lower Silurian Longmaxi Shale, upper Yangtze region, China. Int. J. Coal Geol. 128–129, 1–11. https://doi.org/10.1016/j.coal.2014.03.004.
Keller, J.M., Chen, S., Crownover, R.M., 1989. Texture description and segmentation through fractal geometry. Comput. Vis. Graph. Image Process. 45, 150–166. https://doi.org/10.1016/0734-189X(89)90130-8.
Klein, J., Perahia, D., Warburg, S., 1991. Forces between polymer-bearing surfaces undergoing shear. Nature 352, 143–145. https://doi.org/10.1038/352143a0.
Kolařk, J., 1998. Simultaneous prediction of the modulus, tensile strength and gas permeability of binary polymer blends. Eur. Polym. J. 34, 585–590. https://doi.org/10.1016/S0014-3057(97)00176-6.
Krohn, C.E., Thompson, A.H., 1986. Fractal sandstone pores: automated measurements using scanning-electron-microscope images. Phys. Rev. B 33, 6366–6374. https://doi.org/10.1103/PhysRevB.33.6366.
Le, T., Le Saout, G., Garcia-Diaz, E., Betrancourt, D., Rémond, S., 2017. Hardened behavior of mortar based on recycled aggregate: Influence of saturation state at macro- and microscopic scales. Constr. Build. Mater. 141, 479–490. https://doi.org/10.1016/j.conbuildmat.2017.02.035.
Liu, K., Ostadhassan, M., 2017. Multi-scale fractal analysis of pores in shale rocks. J. Appl. Geophys. 140, 1–10. https://doi.org/10.1016/j.jappgeo.2017.02.028.
Luchnikov, V.A., Gavrilova, M.L., Medvedev, N.N., Voloshin, V.P., 2002. The Voronoi–Delaunay approach for the free volume analysis of a packing of balls in a cylindrical container. Futur. Gener. Comput. Syst. 18, 673–679. https://doi.org/10.1016/S0167-739X(02)00032-8.
Milutinović-Nikolić, A., Talijan, N., Jeremić, K., Aleksić, R., 2002. Optical fibers with composite magnetic coating. Mater. Lett. 56, 148–155. https://doi.org/10.1016/S0167-577X(02)00431-7.
Mitić, V.V., Paunović, V., Janković, S., Pavlović, V., Antolović, I., Rančić, D., 2013. Electronic ceramic structure within the Voronoi cells model and microstructure fractals contacts surfaces new frontier applications. Sci. Sinter. 45, 223–232. https://doi.org/10.2298/SOS1302223M.
Pegg, E.C., Gill, H.S., 2016. An open source software tool to assign the material properties of bone for Abaqus finite element simulations. J. Biomech. 49, 3116–3121. https://doi.org/10.1016/j.jbiomech.2016.07.037.
Poomalai, P., Ramaraj, B., Siddaramaiah, 2007. Poly(methyl methacrylate) toughened by ethylene-vinyl acetate copolymer: physico–mechanical, thermal, and chemical properties. J. Appl. Polym. Sci. 104, 3145–3150. https://doi.org/10.1002/app.25879.
Russell, S., Walker, D.M., Tordesillas, A., 2016. A characterization of the coupled evolution of grain fabric and pore space using complex networks: pore connectivity and optimized flows in the presence of shear bands. J. Mech. Phys. Solids 88, 227–251. https://doi.org/10.1016/j.jmps.2015.12.009.
Stach, S., Lamża, A., Wróbel, Z., 2014. 3D image multifractal analysis and pore detection on a stereometric measurement file of a ceramic coating. J. Eur. Ceram. Soc. 34,

3427–3432. https://doi.org/10.1016/j.jeurceramsoc.2014.04.008.
Tomić, N.Z., Dimitrijević, M.M., Međo, B.I., Rakin, M.P., Jančić Heinemann, R.M., Radojević, V.J., Aleksić, R.R., 2014. Comparison of mechanical behavior of SiC sintered specimen to analysis of surface defects. Sci. Sinter. 46. https://doi.org/10.2298/SOS1402225T.
Tomić, N.Z., Međo, B.I., Stojanović, D.B., Radojević, V.J., Rakin, M.P., Jančić-Heinemann, R.M., Aleksić, R.R., 2016. A rapid test to measure adhesion between optical fibers and ethylene–vinyl acetate copolymer (EVA). Int. J. Adhes. Adhes. 68, 341–350. https://doi.org/10.1016/j.ijadhadh.2016.04.012.
Tomić, N.Z., Veljović, Đ., Trifković, K., Međo, B., Rakin, M., Radojević, V., Jančić-Heinemann, R., 2017. Numerical and experimental approach to testing the adhesive properties of modified polymer blend based on EVA/PMMA as coatings for optical fibers. Int. J. Adhes. Adhes. 73, 80–91. https://doi.org/10.1016/j.ijadhadh.2016.11.010.
Tucker III, C.L., Moldenaers, P., 2002. Microstructural evolution in polymer blends. Annu. Rev. Fluid Mech. 34, 177–210. https://doi.org/10.1146/annurev.fluid.34.082301.144051.
Visakh, P.M., Markovic, Gordana, Pasquini, Daniel, 2016. Recent Developments in Polymer Macro, Micro and Nano Blends. Woodhead Publishing.
Voloshin, V.P., Kim, A.V., Medvedev, N.N., Winter, R., Geiger, A., 2014. Calculation of the volumetric characteristics of biomacromolecules in solution by the Voronoi–Delaunay technique. Biophys. Chem. 192, 1–9. https://doi.org/10.1016/j.bpc.2014.05.001.
Wang, J., Lessard, B.H., Maric, M., Favis, B.D., 2014. Hierarchically porous polymeric materials from ternary polymer blends. Polymer (Guildf) 55, 3461–3467. https://doi.org/10.1016/j.polymer.2014.06.042.
Xie, H., Wang, J., 1999. Direct fractal measurement of fracture surfaces. Int. J. Solids Struct. 36, 3073–3084. https://doi.org/10.1016/S0020-7683(98)00141-3.
Zambrano, M., Tondi, E., Mancini, L., Arzilli, F., Lanzafame, G., Materazzi, M., Torrieri, S., 2017. 3D pore-network quantitative analysis in deformed carbonate grainstones. Mar. Pet. Geol. 82, 251–264. https://doi.org/10.1016/j.marpetgeo.2017.02.001.
Zebarjad, S.M., Sajjadi, S.A., Sdrabadi, T.E., Sajjadi, S.A., Yaghmaei, A., Naderi, B., 2011. A study on mechanical properties of pmma/hydroxyapatite nanocomposite. Engineering 3, 795–801. https://doi.org/10.4236/eng.2011.38096.